J Mater Sci (2011) 46:1685–1696
DOI 10.1007/s10853-010-4986-2

Time-dependent reinforcement effect of nanoclay in rubber nanocomposites

H. H. Le · Z. Ali · S. Ilisch · H.-J. Radusch

Received: 16 August 2010 / Accepted: 6 October 2010 / Published online: 20 October 2010

Abstract The time-dependent reinforcement of rubber–clay composites was characterized by means of stress relaxation experiments combined with a new evaluation method based on the two-component model. The total reinforcement effect of clay in rubber composites was considered as the sum of several stress components, which are originated by different networks. By means of this new experimental strategy a structural characterization of the stress relaxation behavior was performed by taking into account the effect of the degree of clay dispersion. The time-independent reinforcement component determined by the chemical cross-linking density of the rubber matrix decreases with the increased degree of clay dispersion, because the cross-linking process is hindered due to the spatial effect of the clay platelets. The increase of the time-dependent reinforcement component is determined by the development of the bonded rubber layer at the filler surface and the formation of the clay network, which in turn depends on the degree of intercalation and exfoliation of the clay.

Introduction

Nanocomposites on the basis of polymer and highly anisotropic nanoclay have gained considerable attention because of their exceptional thermal, barrier, and mechanical properties. A high degree of intercalation and exfoliation of the nanoclay to expose the large available surface area to the host matrix and increase the effective aspect ratio of the nanoclay particles is the key aspect for the improvement of the composite performance [1]. A large number of studies have been done for characterization of the effect of microstructure of clay and its dispersion state on the time and temperature dependence of flow behavior and the correlated reinforcement of thermoplastics–clay nanocomposites [2–10]. Over the past decade, clay nanocomposites on the basis of rubbers have been frequently developed [11–23]. Considerable efforts have been undertaken to understand the reinforcement mechanisms of rubber–clay nanocomposites. Several experimental and theoretical studies have claimed that the polymer–filler interaction is the only factor that is responsible for reinforcing the polymer nanocomposites [24–28]. Moreover, Schön et al. [21] used mechanical and dynamic mechanical analysis methods to emphasize the role of filler–filler network of nanoclay for reinforcing solution styrene butadiene rubber (SSBR) composites and found that filler networking can be achieved by organoclay with a much lower loading compared to silica or carbon black due to the highly anisotropic platelet-like structure of the organoclay aggregates. Heinrich et al. [19, 20, 23] found a considerable effect on dynamic properties during strain sweep analysis of nanocomposites based on carboxylated nitrile rubber (XNBR) and organoclay, which was attributed to the failure of clay network according to the 'Payne'-like effects. Carretero-Gonzalez et al. [18] used broadband dielectric spectroscopy and in situ synchrotron wide-angle X-ray diffraction to characterize the molecular structure of the polymer network of NR-clay nanocomposites and their morphological changes during deformation. It was found that the presence of nanoclay introduces a dual

H. H. Le (✉) · S. Ilisch · H.-J. Radusch
Center of Engineering Sciences, Polymer Technology,
Martin Luther University Halle-Wittenberg, Kurt-Mothes-Str. 1,
06099 Halle, Germany
e-mail: hai.le.hong@iw.uni-halle.de

Z. Ali
Department of Chemical Engineering, COMSATS Institute
of Information Technology, Defence Road off Raiwind Road,
Lahore, Pakistan

crystallization mechanism due to the alignment of nanoparticles during stretching. The improved reinforcement in NR-clay nanocomposites can be attributed to a super-network structure containing chemically cross-linked chains, nanofiller, and physical networks made by crystallizable chains. Ganter et al. [22] and Giannelis et al. [28, 29] attributed the mechanical property enhancement of NR-clay nanocomposites to the nanoparticle mobility and orientation during deformation. They also suggested that the presence of nanoparticles introduces new energy-dissipating mechanisms causing enhanced hysteresis. A study made by Joly et al. [30] using birefringence and infrared dichroism on NR-clay nanocomposites also reported a higher orientation of amorphous chains by the addition of nanoclays. However, up to date only few studies reported about the time- and temperature-dependent reinforcement of rubber–clay nanocomposites [20, 23, 31]. Compared to the thermoplastics–clay composites the rubber–clay nanocomposites have to undergo a cross-linking process before receiving their end-used state. As results of this process, not only the molecular mobility of rubber chains is altered but also the clay dispersion and orientation becomes significantly changed [15–17]. Fritzsche and Heinrich [20, 23] used dielectric measurements and detected three relaxation processes in XNBR–clay nanocomposites in microscopic and *sub*-microscopic scales. The relaxation process at low temperatures could be assigned to the γ-process due to the rotational motion of side groups. Its temperature dependence follows an Arrhenius-like behavior, and there is no significant change in the shape of this process with the incorporation of filler. The glass transition at medium temperature shows a Vogel–Fulcher dependence but seems to be independent of filler as well. At higher temperatures a new relaxation process was detected, which is probably due to Maxwell–Wagner polarization of mobile ions at the surface or inside the filler, which covers the zinc-carboxyl cluster process [20, 23]. The dynamic mechanical high temperature loss process is probably also due to the thermal decay of zinc-carboxyl clusters. Alternatively, it may result from movement and sliding processes of the anisotropic clay aggregates, which are not occurring with silica as reinforcing filler or it is based on the change of the polymer dynamics close to filler surfaces, which seem to be highly different in organoclay-filled samples compared to silica as reinforcing filler. Apparently, such microscopic relaxation processes lead to a time and temperature dependence of deformation behavior and reinforcement effect of rubber nanocomposites in macroscopic scale. Concerning this issue in this study the stress relaxation experiment was conducted in order to characterize the time-dependent reinforcement of the rubber–clay nanocomposites. Among different models used for evaluation of the stress relaxation curves the two-component model has been frequently used. On its basis the relaxation curve $\sigma(t)$ can be separated into two components, a relaxing curve $\Delta\sigma(t)$ and a non-relaxing stress component σ_∞ [32–35]:

$$\sigma(t) = \Delta\sigma(t) + \sigma_\infty \tag{1}$$

If $t \to \infty$, the initial stress value σ is the sum of the relaxing stress component $\Delta\sigma$ and the non-relaxing stress one σ_∞:

$$\sigma = \Delta\sigma + \sigma_\infty \tag{2}$$

According to Seeger [32, 33] the relaxing stress component $\Delta\sigma$ is called thermally activated stress component, because it acts on short-range obstacles, which can be overcome by stress-aided thermal activation. It depends on the plastic deformation rate and temperature according to Eyring's rate theory [34]. In contrast to the relaxing stress component $\Delta\sigma$, the non-relaxing stress component σ_∞ is called athermal stress component. It is originated from long-range stress fields, which cannot be overcome by thermal activation. The two-component model was successfully applied for evaluating the time- and temperature-dependent deformation behavior of unfilled thermoplastic elastomers (TPE) [36], oil extended TPE [37], carbon black (CB)-filled rubber composites [38], and CB filled TPE [39].

Regarding the micro- and nanostructure of clay in rubber composites, recently, the wetting concept [40] and the methods of the online measured electrical conductance [41, 42] delivered comprehensive knowledge about the wetting behavior of filler surface, the infiltration processes of the rubber chains into the filler agglomerate voids, and the dispersion kinetics of filler agglomerates as well as the development of the filler network during the mixing process. The characterization of the effect of morphology development on the stress relaxation behavior of the rubber–clay nanocomposites by use of the two-component model is the focus of this study.

Materials and experimental

Materials

Carboxylated hydrogenated nitrile butadiene rubber (XHNBR) Therban XT VP KA 8889 (Lanxess) with acrylonitrile content of 33 wt% was used as host polymer. Organoclay Nanofil 9 (Süd-Chemie) modified by stearyl benzyl dimethyl ammonium chloride with layer spacing of 2.0 nm, an average particle size of about 35 μm, and a weight loss on ignition of 35 wt% was used as filler. Peroxide Luperox 101 (Atofina Chemicals) was used as cross-linking agent.

XHNBR was mixed with peroxide in an internal mixer PolyLab System Rheocord (Thermo Electron/Haake) at an initial chamber temperature of 50 °C and a rotor speed of

70 rpm. Clay was added after 7 min. A clay concentration of 5 wt% was kept constant for all nanocomposites. An unfilled vulcanizate (V) was prepared as a reference sample. A conductivity sensor has been installed in the chamber of the internal mixer to measure the electrical conductivity signal of the mix volume between the sensor and the chamber wall as used in [41, 42]. The construction and position of the conductivity sensor were modified correspondingly in order to detect the conductance signal of the investigated system. Figure 1 depicts the development of the online conductance when adding nanoclay into the XHNBR rubber matrix. The mixing time indicated in this figure is the time after nanoclay addition. The conductance of mixture increases significantly and passes through two distinct points which are assigned as the characteristic point 1 (CP 1) at 4 min and characteristic point 2 (CP 2) at 12 min before it reaches a plateau. In the stage up to CP 1, a sharp increase of the conductance is observed. The development of the conductance declines in the stage between CP 1 and CP 2. After CP 2 no change of the conductance is observed. According to our previous study [12, 43, 44] the increase of the conductive signal after adding nanoclay is attributed to the ionic conduction caused by the free release of the quaternary ammonium ions from the clay galleries. The more the contact area between nanoclay and rubber increases along the mixing time because of the running intercalation and exfoliation processes, the more charge carriers release the clay galleries and impart the matrix a higher electrical conductance. In order to receive rubber–clay composites with defined clay dispersion, the mixing time was varied by taking into account the electrical conductance–time characteristics as done in our previous study [45]. Four samples X-1m, X-4m, X-12m, and X-25m were prepared with mixing time of 1 min, 4 min (at CP 1), 12 min (at CP 2), and 25 min, respectively. After discharge from the mixer,

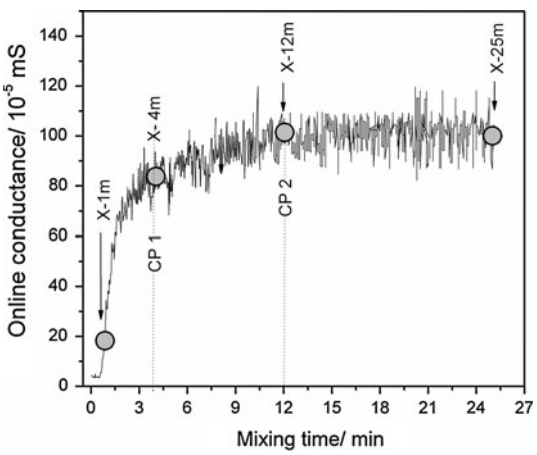

Fig. 1 Online conductance in dependence on mixing times

all samples were cross-linked at a temperature of 150 °C and pressure of 70 bar and t_{90} using a compression molding device P200 (Collin) to get sheets of 0.5 mm thickness for stress relaxation experiments.

Atomic force microscopy

Investigations of microdispersion were carried out by a Universal Scanning Probe Microscope (AFM) (Ambios), operated in intermittent mode with a scan-head of 5 µm. Samples were produced by cutting in a cryo-chamber CN 30 of a rotary microtom HM 360 (Microm) with a diamond knife at −120 °C.

X-ray diffraction

Small-angle X-ray scattering (SAXS) measurements were performed at room temperature using a rotating anode X-ray source RU-3HR (Rigaku) equipped with an X-ray optics device (Confocal Max-Flux, $\lambda = 0.154$ nm, Osmic Inc.) and a Bruker Hi-Star 2-D detector for detection of the state of exfoliation. The generator voltage was 40 kV and generator current was 60 mA. The scattering vector q is defined by $q = 4\pi/\lambda \sin\theta$. All samples had a uniform thickness of 0.5 mm, i.e., the obtained peak area corresponds to the amount of ordered structures.

Extraction experiments of uncured mixtures for determination of the rubber-layer L bonded on the surface of nanoclay

On the basis of our developed method [40] the characterization of the wetting behavior of nanoclay by rubber chains was realized. When nanoclay is mixed with a rubber, a part of the rubber chains will be bonded to the existing reactive groups, which are available on the surface of nanoclay. The bound rubber cannot be separated from the filler when the filled compound is extracted in a good solvent, such as acetone, during a certain period of time. The larger the amount of rubber that stays on the clay surface, the better the polymer–filler interaction, which has also been related to improved final properties. The interactions which keep the polymer on the filler surface can be explained from two different views: On the one hand, bound rubber has been regarded to be caused merely by adsorption effects in which van der Waals forces and chemisorption play the main role [46]. On the other hand, bound rubber formation has been attributed to a chemical process. This process was assumed to be caused by reactions of the rubber with functional groups present on the surface of filler [47]. Also rubber radicals formed by mechanical-chemical degradation during mixing can react with active sites newly formed on filler, for example due to the breakdown of its structure during mixing

[48]. Extracting the unvulcanized rubber compounds with acetone, the bound part of the rubber forming a layer on the clay surface remains in the rubber-filler gel. The determination of the amount of rubber-layer L bound to the surface of the nanoclay was carried out according to Eq. 3 [40].

$$L = \frac{m_2 - m_1 \cdot c_R}{m_2} \tag{3}$$

The mass m_1 corresponds to the rubber compound before extracting; it is the sum of the mass of the undissolvable rubber, the mass of the soluble rubber, and of nanoclay. m_2 is the mass of the rubber-filler gel, which is the sum of the undissolvable rubber and the mass of nanoclay. c_R is the mass concentration of nanoclay in the mixture. For the experimental work 0.25 g of the uncured mixture was stored at room temperature in 100 ml acetone. After 3 days, the rubber-filler gel was taken out and dried up to a constant mass.

Swelling experiments of cured vulcanizates and composites

Swelling experiments were performed with cured samples by equilibrating them in acetone at room temperature for 48 h. As the weight fraction of clay of 5 wt% is considered as negligible, the swelling degree Q and the cross-linked part C were simply calculated using the Eq. 4.

$$Q = \frac{W_{sw} - W_i}{W_{dr}} \times 100\%; \quad C = \frac{W_{dr}}{W_i} \times 100\% \tag{4}$$

where W_i is the weight of the rubber sample before immersion into the solvent, W_{sw} and W_{dr} are the weights of the sample in the swollen state and after drying in an oven at 80 °C for 2 h from its swollen state, respectively.

Stress relaxation experiments

Stress relaxation experiments were performed using a testing machine 1425 with a 2 kN measuring head (Zwick/Roell). The machine was equipped with a heating chamber enabling a long-term constancy of the temperature. Relaxation curves for all samples were recorded at a draw ratio $\lambda = 1.5$ (strain $\varepsilon = 50\%$) within the temperature range from 30 to 110 °C over a period of about 3 h. A strain rate of 100% min^{-1} was kept constant. No steady state of stress values was observed even after 3 h. Therefore, an extrapolation method proposed by Li [49] was used to determine the non-relaxing stress component σ_∞.

Results and discussion

Characterization of the morphology development of the rubber–clay nanocomposites along the mixing time

The course of the wetting process of the clay surface by the rubber chains is expressed by the values of the rubber-layer L in Fig. 2a together with the online conductance curve. According to the discussion made by Manas-Zloczower [50, 51] about the infiltration and dispersion processes, rubber molecules first infiltrate the outer layer of clay agglomerate and wet the clay surface and then intercalate the clay galleries. This clay layer is then peeled off and a new clay surface is created. The new clay surface is progressively wetted by the rubber. As a result, the wetting, intercalating, and dispersion take place simultaneously during the mixing process. The fast increasing rubber-layer L observed in Fig. 2a indicates that the rubber chains diffuse very fast into the clay galleries and intercalate them. At CP 1 the rubber-layer L reaches a plateau, indicating that all the interlayer spacings of clay are fully intercalated, although the exfoliation process is not yet completed.

The SAXS analysis in Fig. 2b shows curves of the nanocomposites with large broad peaks representing the interlayer spacing of the nanoclay in the nanocomposites. While they are changed in intensity with increasing mixing time, the position of the peaks, however, remains unchanged. The data of the clay provider as well as own

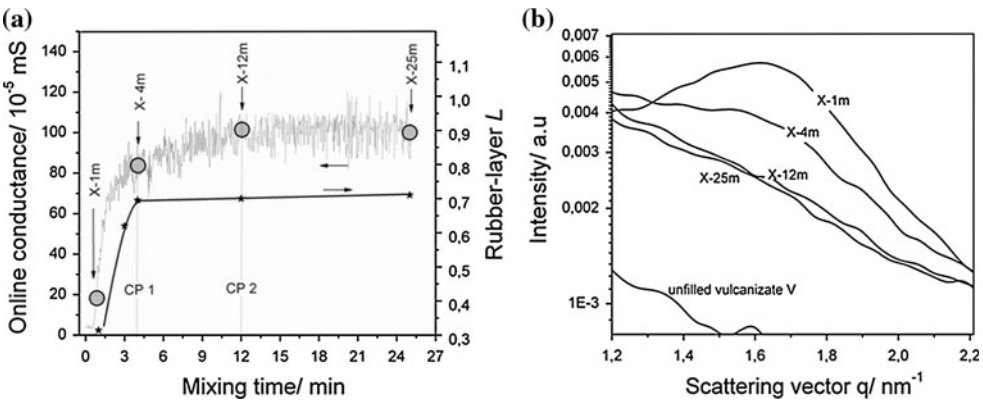

Fig. 2 Online conductance and rubber-layer L in dependence on mixing times (**a**), and SAXS curves of different samples (**b**)

investigations show that the organoclay has a basal spacing of 2.0 nm before compounding. The characteristic peak at the scattering vector $q = 1.59$ nm^{-1} corresponds to a basal spacing of about 4.3 nm of the organoclay in the nanocomposites. As the mixing time increases, the peak height decreases. The peak reaches the highest level after a mixing time of about 1 min for sample X-1m due to the intercalation process. The following decrease of the peak height indicates that the regular structure in the nanocomposite is collapsed, i.e., the nanoclay is exfoliated in the polymer matrix. As discussed above (Fig. 2a) the intercalation process runs mainly up to CP 1. Thus, we can conclude that in sample X-4m both intercalated and exfoliated state available and they affect the height of the peak in the opposite direction. In the stage between CP 1 (sample X-4m) and CP 2 (sample X-12) only the exfoliation process runs and causes a moderated increase of the online conductance since the release of the ionic species is more convenient. The disappearance of the peak in the SAXS curve behind CP 2 indicates a constant morphology of fully exfoliated state in sample X-12m and X-25m, respectively, which causes a constant conductance in this period (Fig. 2a).

The microdispersion of organoclay in rubber was characterized by AFM and is presented in Fig. 2. After mixing time of 1 min large clay tactoids are visible in Fig. 3a for sample X-1m. Both intercalated and exfoliated structures are presented in Fig. 3b for sample X-4m. In the period between CP 1 and CP 2 the number of separated nanolayers increases due to the exfoliation process. As visible in Fig. 3c for sample X-12m only separate clay platelets are observed. The same morphology was obtained for sample X-25m (not shown) that supports the constant value of the online conductance after CP 2.

Concerning the clay dispersion in NBR composites Sahdu [52] using TEM and AFM technique could show that hydrogenated acrylonitrile butadiene rubber (HNBR) forms with clay intercalated and exfoliated structures both with the unmodified and the modified clay. Kim [53] investigated the effect of the chain length (number of carbon atoms) of the surfactant on the clay dispersion in HNBR and found that clay modified with C8-surfactants shows an intercalated structure, meanwhile C12- and C18-surfactants modified clay exfoliates fully in NBR. Several authors [11–14] reported also that the presence of carboxyl groups on NBR leads to a total exfoliated state of clay composites.

The cross-link density of the rubber matrix of the investigated samples can be estimated by the swelling degree Q and the cross-linked part C of the rubber matrix as shown in Fig. 4.

The swelling degree Q of about 375 wt% was found for the unfilled vulcanizate V. It increases slightly with the improvement of clay dispersion. However, for rubber–clay nanocomposites, an increase of Q cannot finally be concluded as a decrease of the cross-linking density of the matrix. It was found that the solvent uptake ability of the clay nanocomposites increases with respect to the neat rubber due to the presence of alkyl ammonium cations [54]. The influence of the unmodified nanoclay on the curing kinetics of sulfur-cured clay–rubber nanocomposites was investigated by Das et al. [55]. It is apparent that the curing rate is significantly reduced in filled compounds as compared to gum compound. Therefore, it can be said that the presence of the unmodified nanoclays causes partial inactivation of the curatives. They speculated that clay interacts with ethylene thiourea through hydrogen bonding between electronegative oxygen of the clay layers and hydrogen atom, attached with the nitrogen atom of thiourea. For the modified clay–rubber nanocomposites the

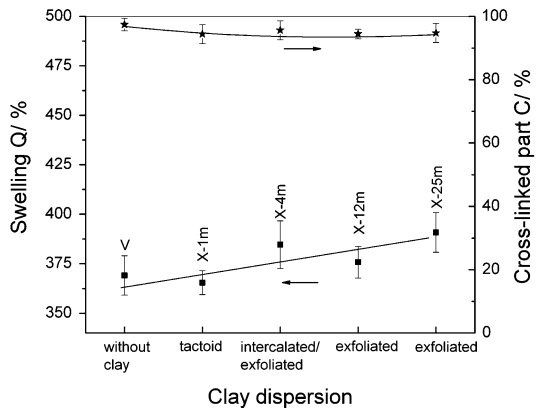

Fig. 4 Swelling degree Q and cross-linked part C of the unfilled vulcanizate V and the composites

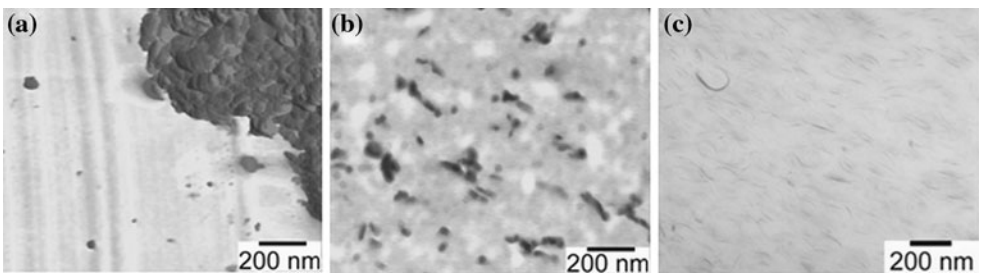

Fig. 3 Microdispersion of investigated samples, X-1m (**a**), X-4m (**b**), and X-12m (**c**)

possible formation of a Zn-complex, in which sulfur and ammonium modifier participate may facilitate for the increase in rate of cure [11, 56]. However, no article reported about the effect of nanoclay on the cure behavior of peroxide-cured clay–rubber composites as presented in this study.

Stress relaxation behavior

The stress relaxation curves of the unfilled vulcanizate *V* and composite X-25m recorded at 50 °C are shown in Fig. 5a. Addition of nanoclay reinforces the rubber matrix and thus the value of the initial stress σ^{Comp} of the composite at the beginning of the relaxation experiment lies at a higher level compared to σ^{V} of the unfilled vulcanizate. It is remarkable that the curve $\sigma^{\mathrm{Comp}}(t)$ intersects the curve $\sigma^{\mathrm{V}}(t)$ after a certain time of relaxation. By neglecting the chemical chain scission the stress will theoretically reach an end-value, i.e., the non-relaxing stress $\sigma_{\infty}^{\mathrm{Comp}}$ and σ_{∞}^{V} at the infinite time t_{∞} as indicated in Fig. 5a.

In order to determine the non-relaxing stress σ_{∞} an extrapolation method proposed by Li [49] was used. He proposed that the relaxation rate $-\mathrm{d}\sigma/\mathrm{dlog}t$ becomes zero at the infinite time when all relaxation processes are finished. The determination of σ_{∞} from the relaxation curves according to the principle of this method is representatively shown in Fig. 5b. In a diagram $-\mathrm{d}\sigma/\mathrm{dlog}t$ vs. σ the extrapolation of the straight part of the curves toward the *x*-axis intersects it at a certain value, which is identified as σ_{∞}. Unexpectedly, the value of the non-relaxing stress $\sigma_{\infty}^{\mathrm{Comp}}$ is significantly lower than that of σ_{∞}^{V}, which means that the reinforcement of nanoclay not only disappears after a certain relaxation period, but also the composite in fact becomes softer than the unfilled vulcanizate.

On the basis of the two-component model we have developed an evaluation method for the characterization of the stress relaxation behavior of multi-component polymer systems [38, 40]. The basic idea is to consider the investigated system as a combination of different networks. A systematic variation of material parameters and test conditions allows separating the initial stress σ into different components and to assign them to the according networks in the system. The relaxing stress component $\Delta\sigma^{V}$ is originated by the relaxation process of the entanglements (slip-link). In the entropy elastic state above the glass transition temperature the relaxing stress component $\Delta\sigma^{V}$ decreases with increasing test temperature (Fig. 6a), because the relaxation process is thermally accelerated and as a result a part of relaxation process takes place already during the stretching period. The non-relaxing stress σ_{∞}^{V} is related to the chemically cross-linked network of the rubber. With increasing test temperatures the non-relaxing stress σ_{∞}^{V} increases slightly (Fig. 6a) that has been explained by means of the entropy elasticity theory [57]. By addition of nanoclay into the rubber matrix the relaxing stress shifts to a higher level, while the non-relaxing stress shifts to a lower level at all test temperatures as seen in Fig. 6a. It is apparent from this result that the reinforcement of nanoclay is resulted from an increasing value of the time-dependent component $\Delta\sigma^{\mathrm{Comp}}$, which is relaxed toward zero at $t = \infty$, and a decreasing value of the time-independent one $\sigma_{\infty}^{\mathrm{Comp}}$. This fact explains why nanoclay shows a negative effect with respect to the reinforcement after a long relaxation period as seen in Fig. 5a.

In Fig. 6b the non-relaxing stress $\sigma_{\infty}^{\mathrm{Comp}}$ and the relaxing stress $\Delta\sigma^{\mathrm{Comp}}$ measured at different temperatures are presented in dependence on the clay dispersion state. In general, it is obvious that $\sigma_{\infty}^{\mathrm{Comp}}$ decreases with better clay dispersion and $\Delta\sigma^{\mathrm{Comp}}$ increases. When clay is just incorporated into the rubber matrix at very short mixing time (sample X-1m) both stress components nearly remain unchanged compared to that of the unfilled vulcanizate *V*. The change of $\sigma_{\infty}^{\mathrm{Comp}}$ and $\Delta\sigma^{\mathrm{Comp}}$ is strong when the clay dispersion goes from tactoid state of X-1m to intercalated/exfoliated state of X-4m. Only a small change of both stress components was observed between X-4m and X-12m, when the clay dispersion goes from intercalated/exfoliated state to the fully exfoliated state. Both composites X-12m and X-25m having the same morphology show insignificant difference in $\sigma_{\infty}^{\mathrm{Comp}}$ and $\Delta\sigma^{\mathrm{Comp}}$, respectively.

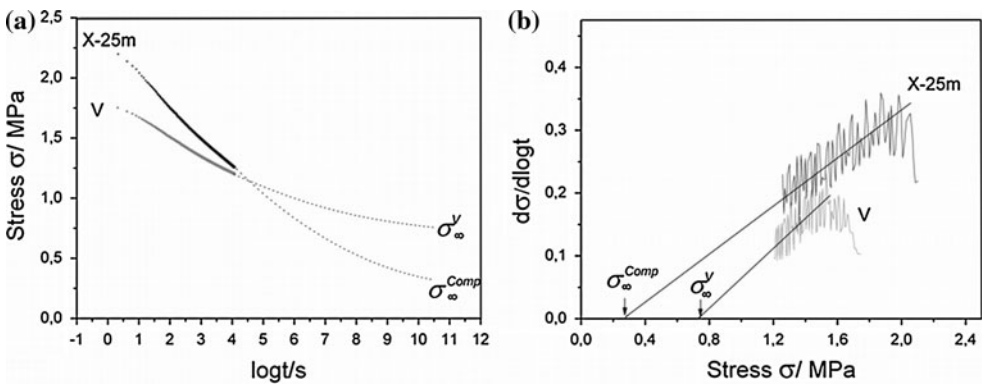

Fig. 5 Stress relaxation curves of the unfilled vulcanizate *V* and the composite X-25m recorded at 50 °C (**a**), and experimental determination of the non-relaxing stress σ_{∞} (**b**)

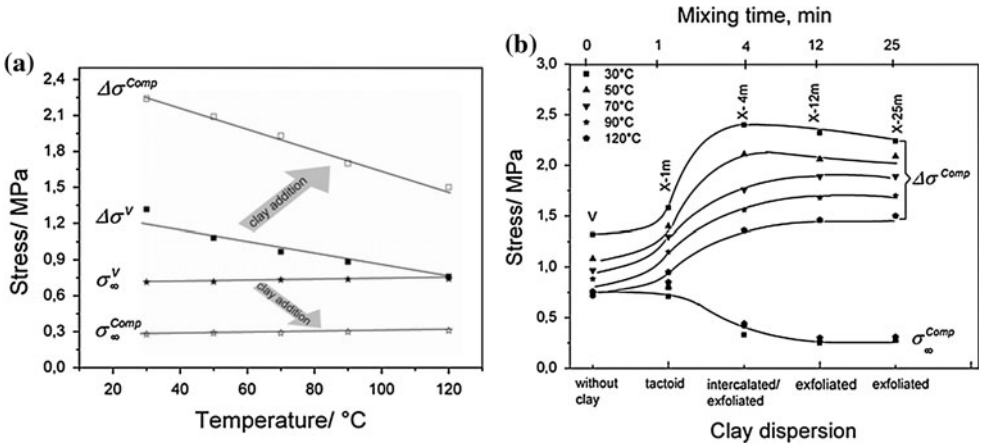

Fig. 6 Non-relaxing stress σ_∞ and relaxing stress $\Delta\sigma$ of the unfilled vulcanizate *V* and the composite X-25m, respectively, in dependence on the test temperatures (**a**) and clay dispersion state (**b**)

The physical background of the experimental results of this study could be discussed by taking into account the formation of different networks in the nanocomposites as illustrated schematically in Fig. 7. The attribution of the stress components $\sigma_\infty^{\mathrm{Comp}}$ and $\Delta\sigma^{\mathrm{Comp}}$ to the networks could be discussed on the basis of the results in our previous study reported about the stress relaxation behavior of carbon black-filled rubber composites [38].

In the composite X-1m the incorporated clay tactoids are isolated in the rubber matrix, which consists of a network of chemical cross-links and a physical network of slip-links (Fig. 7a). In this bad dispersion state, the contact area between rubber and clay is insignificant, and therefore, clay shows only a minimal reinforcement effect. The non-relaxing stress $\sigma_\infty^{\mathrm{Comp}}$ determined by the network of chemical cross-links and the relaxing stress $\Delta\sigma^{\mathrm{Comp}}$ by the physical network of slip-links are corresponding to that of the unfilled vulcanizate.

In the intercalated/exfoliated state of composite X-4m shown in Fig. 7b, rubber gets now a huge contact area with the clay surface. Sadhu et al. [52] reported about possible rubber–clay interaction taking place in rubber–clay nanocomposites. For NBR–clay systems, few OH-groups are present on the surface of the clay, which are possibly capable of forming H-bonds with the –CN groups of the NBR chains. The polymer chains can intercalate inside the galleries and the butadiene part of NBR can interact with the long carbon chains of the clay modifier through some van der Waals forces. Pradhan and Heinrich [58] used FTIR technique and detected also strong polar or even ionic interactions of the polar –CN and acidic –COOH groups of XNBR with the basic –OH functionalities on the clay surface. The extent of H-bond formation depends on the –CN and –COOH content as well as the number of the OH-groups available at the edge of clay platelets. The stable rubber–clay links made by the ionic interactions between –CN/–COOH and OH-groups may additionally contribute to the non-relaxing stress $\sigma_\infty^{\mathrm{Comp}}$ beside the chemical cross-links of the matrix. However, because of a limited number of OH-groups of clay the contribution of strong rubber–clay links to the $\sigma_\infty^{\mathrm{Comp}}$ is considered as negligible. As shown in Fig. 5b $\sigma_\infty^{\mathrm{Comp}}$ decreases strongly when clay is intercalated/exfoliated that is merely related to the reduction of the chemical cross-linking density. Zhu et al. [59] determined a decrease in the cross-link density of the rubber–clay nanocomposites, measured by swelling test. He speculated that the clay in its intercalated state forms a physical network from the clay bundles that

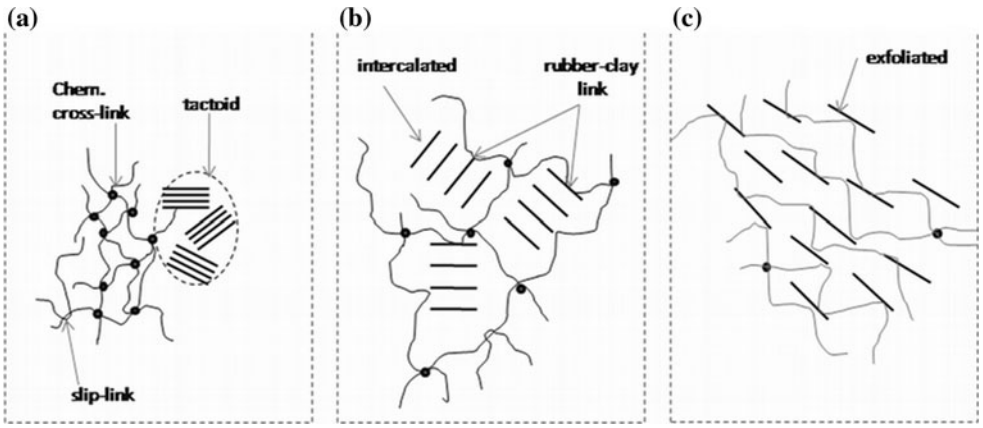

Fig. 7 Networks available in the clay–rubber composite X-1m (**a**), X-4m (**b**), and X-12m (**c**)

simultaneously hinders chemical cross-linking of polymer molecules. The physical interaction between the butadiene part of NBR and the long carbon chains of the surfactants forms instable rubber–clay links. This type of rubber–clay links is time-dependent and resolved during the stress relaxation experiment by the debonding process of rubber molecules from the clay surface. The debonding process, which was simulated and discussed for CB systems [60–62], contributes beside the physical slip-links significantly to the relaxing stress $\Delta\sigma^{\text{Comp}}$. Using dynamic mechanical analysis and dielectric relaxation spectra on CB-filled ethylene–propylene rubber (EPDM) and chlorobutyl vulcanizates Mahapatra and Sirha [63, 64] found that debonding of the rubber chains in the vicinity of filler is essential for stress relaxation behavior.

The increase of the number of rubber–clay links when clay goes from the tactoid state (X-1m) to the intercalated/exfoliated state (X-4m) is evidenced by the increase of the rubber-layer L (Fig. 1a). Additional contribution to $\Delta\sigma^{\text{Comp}}$ can come from the clay–clay interaction in the form of clay bundle edge-to-face interactions, which is resulted from the formation of a so-called ''house of cards'' structure. During relaxation experiment this clay network is ruptured as observed for CB networks discussed in [38, 65].

When clay becomes fully exfoliated the $\sigma_{\infty}^{\text{Comp}}$ went on decreasing as determined for the composite X-12m (Fig. 6b). This result is related to the fact that the separated clay platelets more effectively hinder the chemical cross-linking due to their geometry effect. The slight decrease of $\Delta\sigma^{\text{Comp}}$ is likely caused by the absence of the clay network in the exfoliated state. Das and Heinrich [17] found that the orientation of clay platelets obtained after mixing process is maintained during peroxidic cross-linking, because a lot of cross-linking sites are available for covalent bond formation (C–C), and thus, no conformational rearrangement of molecules is needed for the peroxidic cross-linking process. In contrast, sulfur-cured vulcanizates show a non-oriented isotropy of the platelets. It is assumed that during sulfur curing the conformational rearrangement of the macromolecular chains takes place for providing the sulfur cross-linking sites close together, and in this way the silicate platelets are forced to move along with rubber chains in different directions [15, 16]. The TEM image (Fig. 3c) of the peroxidic-cured composites X-12m shows obviously isotropic-oriented arrangement of clay platelets. Thus, the clay network, which is available in the intercalated X-4m specimen, disappeared in the exfoliated X-12m one.

The non-relaxing stress component σ_{∞}^{V} is caused by the deformation of the network formed by the chemical cross-links. It is related to the molecular weight between two chemical cross-links M_{C} according to the entropy elasticity theory described by Eq. 5 [57] and depends on the draw ratio λ, the density ρ, the Boltzmann constant k, and the absolute temperature T:

$$\sigma_{\infty}^{\text{Comp}} = \left(\lambda - \lambda^{-2}\right)\frac{3\rho kT}{M_{\text{C}}^{\text{cross-link}}} \tag{5}$$

According to the discussion above the relaxing stress $\Delta\sigma^{\text{Comp}}$ is a sum of $\Delta\sigma^{\text{slip-link}}$, $\Delta\sigma^{\text{rubber–clay link}}$, and $\Delta\sigma^{\text{clay–clay link}}$. By assumption that the number of slip-links in the rubber matrix is independent of the clay dispersion state and the contribution of $\Delta\sigma^{\text{clay–clay link}}$ is insignificant the molecular weight between two physical net points $M_{\text{P}}^{\text{slip-link}}$ and $M_{\text{P}}^{\text{rubber–clay link}}$ can be calculated according to Eqs. 6 and 7, respectively:

$$\Delta\sigma^{V} = \Delta\sigma^{\text{slip-link}} = \left(\lambda - \lambda^{-2}\right) \times 3\rho kT\frac{1}{M_{\text{P}}^{\text{slip-link}}} \tag{6}$$

$$\begin{aligned}\Delta\sigma^{\text{Comp}} &= \Delta\sigma^{\text{slip-link}} + \Delta\sigma^{\text{rubber-clay link}} \\ &= \left(\lambda - \lambda^{-2}\right) \times 3\rho kT\left(\frac{1}{M_{\text{P}}^{\text{slip-link}}} + \frac{1}{M_{\text{P}}^{\text{rubber-clay link}}}\right)\end{aligned} \tag{7}$$

The molecular weight between two chemical net points M_{C} and physical net points M_{P} are calculated using Eqs. 5, 6 and 7 and displayed in Fig. 8, respectively, in dependence on the clay dispersion state. $M_{\text{P}}^{\text{slip-link}}$ remains unchanged, while $M_{\text{P}}^{\text{rubber–clay link}}$ decreases strongly when clay intercalated/exfoliated due to the formation of a large number of time-dependent rubber–clay links. When clay is fully exfoliated, $M_{\text{P}}^{\text{rubber–clay link}}$ increases slightly that is related to the fact that the clay bundle network is actually disappeared. $M_{\text{C}}^{\text{cross-link}}$ remains unchanged when clay is only incorporated into the matrix (X-1m) and increases strongly when clay is intercalated/exfoliated (X-4m) and fully exfoliated (X-12m) because of the geometric hindrance of the chemical cross-linking by the clay platelets. It is obvious from Fig. 8 that the time-dependent reinforcement of nanoclay in rubber composites is resulted from the

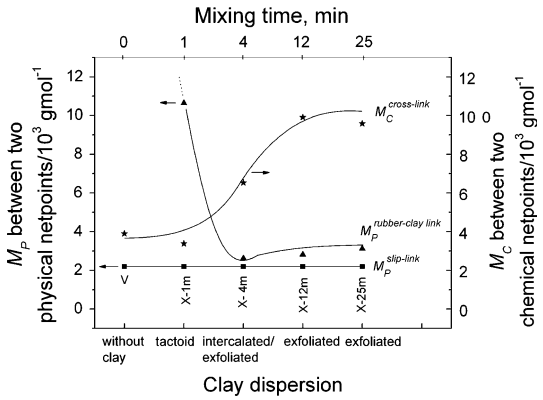

Fig. 8 Molecular weight between two network points M_{P} and M_{C} in different nanocomposites

decrease of the time-independent contribution of the chemical rubber–rubber links and the increase of the time-dependent contribution of physical rubber–clay links.

In order to get better insight into the physical background of the stress components we determined the activation energy of the relaxation processes by means of the generation of the master curve. According to our previous studies [36, 37], the generation of the master curve by horizontal shift of the relaxation curves measured at different test temperature can be applied only for the relaxing stress $\Delta\sigma(t)$. The stress relaxation curves $\sigma(t,T)$ were subtracted by the non-relaxing stress component σ_∞ resulting in the relaxing stress component $\Delta\sigma(t, T)$ according to Eq. 1. As an example, the relaxing stress curves $\Delta\sigma^V(t, T)$ of the unfilled vulcanizate V are presented in Fig. 9a.

By generation of the master curve of the investigated sample the relaxing stress curves $\Delta\sigma^V(t, T)$ were shifted horizontally toward the curve measured at the reference temperature $T_R = 30$ °C as presented in Fig. 9b. The curves measured at different temperatures were well fitted to the reference curve to form a master curve. Fig. 9c and d shows also the well-fitted master curves of the composites X-4m and X-25m, respectively. The horizontal shift factor a_T of all composites was presented in dependence on the reciprocal temperature in Fig. 10. The temperature dependence of log a_T of all investigated samples can be described by the Arrhenius equation [66]. The activation energy $E_A = 40$ kJ/mol of the unfilled vulcanizate V was calculated from the slope of the straight line according to the Arrhenius equation. It is considered as the activation energy of the co-operative rearrangement of rubber chains (slip-link process) and this value is in accordance with results observed by Fritzsche and Heinrich [20] for carboxylated XNBR-clay composites of 45–50 kJ/mol. By means of DMA and dielectrical measurements they could find an additional relaxation process with a low activation energy of 12–15 kJ/mol at temperatures above 50 °C, which was attributed to the new relaxation process taking place in zinc-carboxyl-clusters. In this study, peroxide was used as cross-linking agent and no zinc-carboxyl-clusters

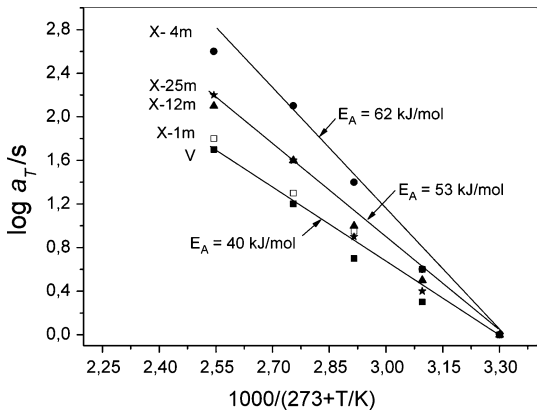

Fig. 10 Temperature dependence of shift factor a_T of unfilled vulcanizate and filled composites

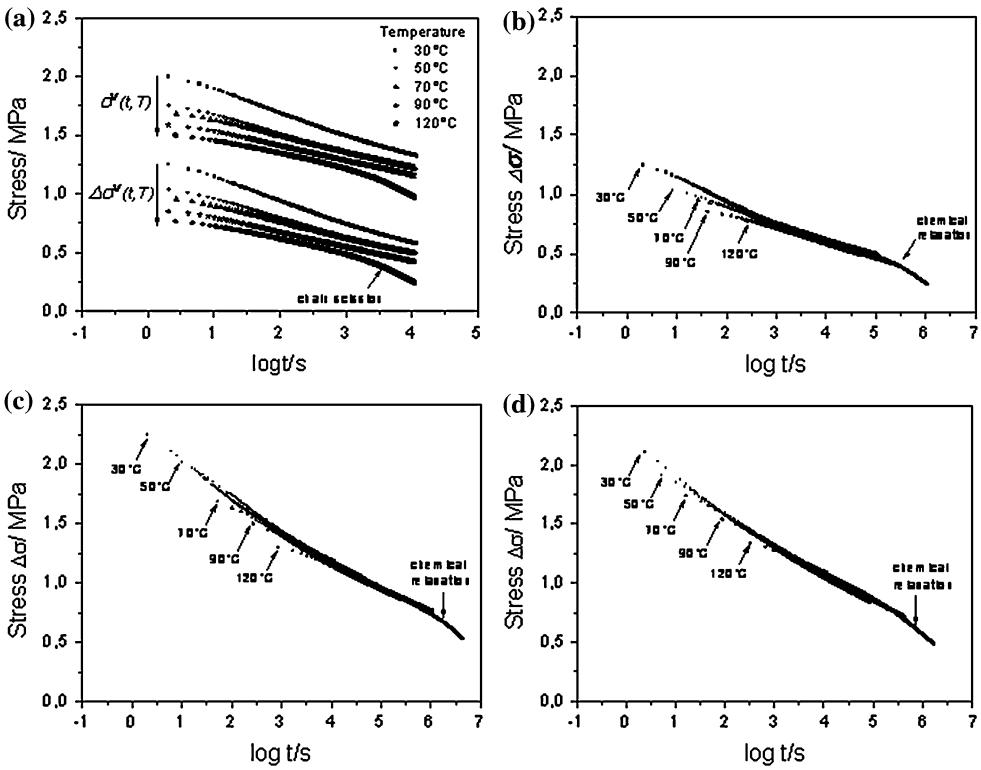

Fig. 9 Stress relaxation curves $\sigma^V(t, T)$ and $\Delta\sigma^V(t, T)$ of the unfilled vulcanizate V recorded at different test temperatures (**a**), master curve created by horizontal shift of the relaxing stress component $\Delta\sigma^V(t, T)$ of the unfilled vulcanizate (**b**) and X-4m (**c**) as well as X-12m (**d**)

could be formed. The composite X-1m showed an activation energy as similar as that of the unfilled sample, because in X-1m clay likely shows no reinforcement effect. Ren et al. [6] found a near independence of the frequency shift factors on the silicate loading and suggested that the temperature-dependent relaxation processes observed in the viscoelastic measurements are essentially unaffected by the presence of the silicate layers. Krishnamoorti et al. [3] obtained a similar activation energy by fitting the data of their tethered poly(ε-caprolactone) PCL-clay nanocomposites and PCL homopolymer over the same temperature range. Since the clay platelets to which the polymers are tethered do not have a temperature-dependent relaxation, the only relaxation process probed as a function of temperature is that of the polymer segments.

An activation energy of 62 kJ/mol was determined for X-4m. Such a high value of activation energy indicates that beside the slip-link process the rupture of the clay network and the debonding process attribute additionally to the relaxing stress $\Delta\sigma^{\text{Comp}}$. Both sample X-12m and X-25m show the same activation energy of 53 kJ/mol, which is lower than that of X-4m and higher than that of X-1m. It is related to the fact that the relaxing stress $\Delta\sigma^{\text{Comp}}$ of X-12m and X-25m is caused by slip-link and debonding processes as discussed before.

In order to compare the reinforcement mechanism of clay with CB in rubber composites we used the data obtained from our previous study [38] reported about stress relaxation behavior of rubber–CB composites and presented them in Fig. 11. Detailed discussion of physical background of $\sigma_{\infty}^{\text{Comp}}$ and $\Delta\sigma^{\text{Comp}}$ of CB-filled composites and their division into different stress components was given in our previous study. Here we would like to show merely the important differences between both types of filler with regard to the reinforcement mechanism. The non-relaxing stress component $\sigma_{\infty}^{\text{Comp}}$ is presented in dependence on the CB macrodispersion, which was determined using the method developed by Stumpe and Railsback [67] and modified by us [45] by evaluating the sample images made by optical microscopy. While $\sigma_{\infty}^{\text{Comp}}$ of clay composites decreases with clay dispersion as discussed in Fig. 6, $\sigma_{\infty}^{\text{Comp}}$ of CB composites shown in Fig. 11a increases with CB dispersion and reaches a maximal value at a dispersion of 91% (composite C91), after that it decays to the same level of C79. On the basis of results obtained from the online measured electrical conductance and measurement of rubber-layer L $\sigma_{\infty}^{\text{Comp}}$ of the CB composites was divided into $\sigma_{\infty}^{\text{cross-link}}$, $\sigma_{\infty}^{\text{rubber–CB link}}$, and $\sigma_{\infty}^{\text{CB–CB link}}$ [38]. In contrast to $\sigma_{\infty}^{\text{cross-link}}$ of clay composites the $\sigma_{\infty}^{\text{cross-link}}$ of CB composites remains not affected by the CB dispersion. It is due to the fact that the presence of CB network does not prevent the chemical cross-linking process because of the porous structure of CB aggregates compared to the plate-like structure of clay. The contributions of $\sigma_{\infty}^{\text{CB–CB link}}$ caused by the strong filler–filler links and $\sigma_{\infty}^{\text{rubber–CB link}}$ caused by the strong rubber–CB links are not negligible compared to $\sigma_{\infty}^{\text{cross-link}}$.

The relaxing stress $\Delta\sigma^{\text{Comp}}$ of CB composites is a sum of $\Delta\sigma^{\text{slip-link}}$, $\Delta\sigma^{\text{rubber–CB link}}$, and $\Delta\sigma^{\text{CB–CB link}}$. The $\Delta\sigma^{\text{slip-link}}$ made by the entanglements remains unchanged with CB dispersion, while $\Delta\sigma^{\text{rubber–CB link}}$ caused by time-dependent rubber–CB links and $\Delta\sigma^{\text{CB–CB link}}$ caused by time-dependent CB–CB links increase significantly when the CB dispersion reaches 79%. Exceeding 79% the contribution of $\Delta\sigma^{\text{rubber–CB link}}$ and $\Delta\sigma^{\text{CB–CB link}}$ remains constant. It is worth to note that at the CB dispersion of 79% the rubber-layer L reaches its level-off value, i.e., CB surface is fully wetted by rubber molecules. According to Fig. 2 the rubber-layer L of clay composites becomes constant for the sample X-4m, and no significant changes of $\Delta\sigma^{\text{rubber–clay link}}$ and $\Delta\sigma^{\text{clay–clay link}}$ are observed in Fig. 6b.

Conclusions

The reinforcement of clay in rubber composites is resulting from time-independent and time-dependent stress components, respectively, which are originated by different

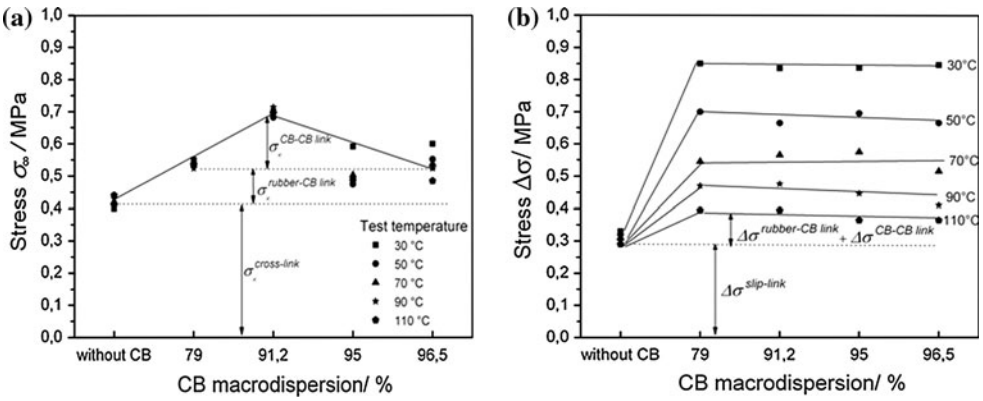

Fig. 11 Non-relaxing stress $\sigma_{\infty}^{\text{Comp}}$ and relaxing stress $\Delta\sigma^{\text{Comp}}$ measured at different temperatures in dependence on the CB macrodispersion [38]

networks. In contrast to rubber–CB composites, in rubber–clay composites the time-independent reinforcement component decreases with clay dispersion degree because of the decrease of chemical cross-linking density of the rubber matrix, while the time-dependent reinforcement component increases significantly with the clay dispersion. The decrease of chemical cross-linking density of the rubber matrix is related to the geometric effect of the clay platelets. The increase of the time-dependent reinforcement component is determined by the development of the rubber-layer L and the formation of clay network, which in turn depends on the degree of intercalation and exfoliation of clay. These results can deliver the basis for a more targeted development and application of rubber–clay composites.

Acknowledgement The authors wish to thank the German Research Foundation (DFG) for the financial support.

References

1. Giannelis EP (1996) Adv Mater 8:29
2. Xu L, Reeder S, Thopasridharan M, Ren J, Shipp DA, Krishnamoorti R (2005) Nanotechnology 16:514
3. Krishnamoorti R, Giannelis EP (1997) Macromolecules 30:4097
4. Krishnamoorti R, Ren J, Silva AS (2001) J Chem Phys 114:4968
5. Krishnamoorti R, Yurekli K (2001) Curr Opin Colloid Interface Sci 6:464
6. Ren J, Silva AS, Krishnamoorti R (2000) Macromolecules 33:3739
7. Horsch S, Serhatkulu G, Gulari E, Kannan RM (2006) Polymer 47:7485
8. Witten TA, Leibler L, Pincus P (1990) Macromolecules 23:824
9. Horsch S, Serhatkulu G, Gulari E, Kannan RM (2006) Polymer 47(21):7485
10. Manitiu M, Bellair RJ, Horsch S, Gulari E, Kannan RM (2008) Macromolecules 41:8038
11. Rajasekar R, Pal K, Heinrich G, Das A (2009) Mater Des 30:3839
12. Ali Z, Le HH, Ilisch S, Busse K, Radusch H-J (2009) J Appl Polym Sci 113:667
13. Wu YP, Zhang LQ, Wang YQ, Liang Y, Yu DS (2001) J Appl Polym Sci 82:2842
14. Ibarra L, Rodrıguez A, MoraIonic I (2007) Eur Polym J 43:753
15. Gatos KG, Sawanis NS, Apostolov AA, Thomann R, Karger-Kocsis J (2004) Macrom Mater Eng 289:1079
16. Gatos KG, Százdi L, Pukánszky B, Karger-Kocsis J (2005) Macromol Rapid Comm 26:915
17. Das A, Jurk R, Stöckelhuber KW, Heinrich G (2007) eXPRESS Polym Lett 1:717
18. Carretero-Gonzalez J, Retsos H, Verdejo R, Toki S, Hsiao BS, Giannelis EP, Lopez-Manchado MA (2008) Macromolecules 41:6763
19. Das A, Jurk R, Stöckelhuber KW, Majumder PS, Engelhardt Th, Fritzsche J, Klüppel M, Heinrich G (2009) J Macrom Sci A 46:7
20. Fritzsche J, Das A, Jurk R, Stöckelhuber KW, Heinrich G, Klüppel M (2008) eXPRESS Polym Lett 2:373
21. Schön F, Gronski W (2003) Kautsch Gummi Kunstst 56:166
22. Ganter M, Gronski W, Reichert P, Mülhaupt R (2007) Rubber Chem Technol 74:221
23. Fritzsche J, Klüppel M (2009) Kautsch Gummi Kunstst 62:16
24. Vilgis TA, Heinrich G (1994) Macromolecules 27:7846
25. Klüppel M (2003) Adv Polym Sci 164:1
26. Gusev AA (2006) Macromolecules 39:5960
27. Sheng N, Boyce MC, Parks DM, Rutledge GC, Abes JI, Cohen RE (2004) Polymer 45:487
28. Shah D, Maiti P, Jiang DD, Batt CA, Giannelis EP (2005) Adv Mater 17:525
29. Shah D, Maiti P, Gunn E, Schmidt DF, Jiang DD, Batt CA, Giannelis EP (2004) Adv Mater 16:1173
30. Joly S, Garnaud G, Ollitrault R, Bokobza L, Mark JE (2002) Chem Mater 14:4202
31. Sridhar V, Chaudhary RNP, Tripathy DK (2006) J Appl Polym Sci 100:3161
32. Seeger A (1958) Handbuch der Physik. Springer, Berlin
33. Seeger A (1954) Z Naturforsch 9a:758, 856, 870
34. Krausz AS, Eyring H (1975) Deformation kinetics. Wiley, New York
35. Ferry JD (1980) Viscoelastic properties of polymers. Wiley, New York
36. Le HH, Lüpke Th, Pham T, Radusch H-J (2003) Polymer 40:4589
37. Le HH, Zia Q, Ilisch S, Radusch H-J (2008) eXPRESS Polym Lett 2:791
38. Le HH, Ilisch S, Radusch H-J (2009) Polymer 50:2294
39. Le HH, Heidenreich D, Kolesov IS, Ilisch S, Radusch H-J (2009) J Appl Polym Sci 117:2622
40. Le HH, Ilisch S, Radusch H-J (2008) Rubber Chem Technol 81:767
41. Le HH, Ilisch S, Jakob B, Radusch H-J (2004) Rubber Chem Technol 77:147
42. Le HH, Prodanova I, Ilisch S, Radusch H-J (2004) Rubber Chem Technol 77:815
43. Ali Z, Le HH, Ilisch S, Radusch H-J (2009) J Mater Sci 44(23):6427. doi:10.1007/s10853-009-3892-y
44. Ali Z, Le HH, Ilisch S, Thurn-Albrecht Th, Radusch H-J (2010) Polymer 51:4580
45. Le HH, Ilisch S, Steinberger H, Radusch H-J (2008) Plast Rubber Compos 37:367
46. Kraus G (1971) Adv Polym Sci 8:155
47. Rivlin D (1971) Rubber Chem Technol 44:307
48. Donnet JB, Voet A (1976) Carbon black, physics, chemistry and elastomer reinforcement. Marcel Dekker, New York Chap 8
49. Li JCM (1967) Can J Phys 45:493
50. Li Q, Feke DL, Manas-Zloczower I (1995) Rubber Chem Technol 68:836
51. Yamada H, Manas-Zloczower I, Feke DL (1997) Rubber Chem Technol 71:1
52. Sadhu S, Bhowmick AK (2005) J Mater Sci 40:1633. doi:10.1007/s10853-005-0663-2
53. Kim J, Oh T, Lee D (2003) Polym Int 52:1058
54. Ratanarat K, Nithitanakul M, Martin DC, Magaraphan R (2003) Rev Adv Mater Sci 5:187
55. Das A, Costa FR, Wagenknecht U, Heinrich G (2008) Eur Polym J 44:3456
56. Kim MS, Kim GH, Chowdhury SR (2007) Polym Eng Sci 47:308
57. Treloar LRG (1975) The physics of rubber elasticity, 3rd edn. Clarendon Press, Oxford
58. Pradhan S, Costa FR, Wagenknecht U, Jehnichen D, Bhowmick AK, Heinrich G (2008) Eur Polym J 44:3122
59. Zhu L, Wool RP (2006) Polymer 47:8106
60. Matouš K, Geubelle PH (2006) Int J Numer Method Eng 65:190
61. Needleman A (1987) J Appl Mech 54:525
62. Lu W, Tomita Y (2004) WCCM VI in conjunction with APCOM'04, 5–10 Sept 2004, Beijing, China
63. Mahapatra SP, Sridhar V, Chaudhary RNP, Tripathy DK (2007) Polym Eng Sci 47:984

64. Sridhar V, Chaudhary RNP, Tripathy DK (2006) J Appl Polym Sci 101:4320
65. Srinivasan N, Bökamp K, Vennemann N (2005) Kautsch Gummi Kunstst 58:650
66. Glasstone S, Laidler KJ, Eyring H (1941) The theory of rate process. McGraw-Hill, New York
67. Stumpe NA, Railsback HE (1964) Rubber World 151:41